Journal of Sound and Vibration 325 (2009) 870–883

Contents lists available at ScienceDirect

Journal of Sound and Vibration

journal homepage: www.elsevier.com/locate/jsvi

Effect of a static force on the dynamic behaviour of a harmonically excited quasi-zero stiffness system

Ivana Kovacic [a,*], Michael J. Brennan [b], Benjamin Lineton [b]

[a] Department of Mechanics, Faculty of Technical Sciences, University of Novi Sad, 21125 Novi Sad, Serbia
[b] Institute of Sound and Vibration Research, University of Southampton, Southampton SO17 1BJ, UK

ARTICLE INFO

Article history:
Received 10 October 2008
Received in revised form
17 March 2009
Accepted 26 March 2009
Handling Editor: M.P. Cartmell
Available online 4 June 2009

ABSTRACT

This paper concerns the way in which a static force can dramatically change the dynamic behaviour of a harmonically excited quasi-zero stiffness single-dof system. The primary resonance response of the system is considered using the harmonic balance method and the results are verified numerically. It is found that the system changes its characteristic from being purely hardening to a mixed softening and hardening characteristic and finally to a purely softening characteristic as the static force increases from zero. Consequently for certain values of the static force multiple jumps can occur. Five different cases of a possible response are distinguished and related to the values of the static force. It is also found that just one harmonic is required to qualitatively describe the behaviour of the system. The inclusion of a second harmonic in the solution does result in changes to the response, especially the softening behaviour, but overall it has a small effect for the system parameters chosen in this paper, which is representative of a quasi-zero stiffness isolator. The influence of damping is also considered.

1. Introduction

A single-dof oscillator with no linear stiffness and with hardening cubic nonlinearity is considered in this paper. Such a stiffness characteristic corresponds to a system with zero dynamic stiffness, a so-called quasi-zero stiffness (QZS) mechanism [1]. QZS mechanisms have wide application. They are used in space research to simulate zero gravity [2], and in geodynamics for seismographs or gravimeters [3,4]. Their use is beneficial for vibration isolation as well [1,5–8].

The equation of motion of the system considered is given by

$$\ddot{y} + 2\zeta\dot{y} + \gamma y^3 = f_0 + f_1 \cos \Omega t, \tag{1}$$

where y, ζ, γ, f_0, f_1 and Ω represent, respectively, the non-dimensional variables of displacement, damping ratio, coefficient of the cubic nonlinearity, constant force and the amplitude and frequency of the harmonic excitation force; overdots denote derivatives with respect to non-dimensional time t.

The mathematical model of this QZS mechanism coincides with the model of an electric circuit, containing an inductor. The nonlinear characteristic of the inductor is such that the relationship between the current and the flux is nonlinear and has the same form as the restoring force in Eq. (1) [9]. While studying this system, but for the case of a fixed value of f_0 and $\gamma = \Omega = 1$, Hayashi [9] showed analytically and confirmed experimentally that multi-valued steady states exist for certain

* Corresponding author. Tel.: +381 214852241; fax: +381 21450207.
E-mail addresses: ivanakov@uns.ac.vs (I. Kovacic), mjb@isvr.soton.ac.uk (M.J. Brennan), bl@isvr.soton.ac.uk (B. Lineton).

0022-460X/$ - see front matter © 2009 Published by Elsevier Ltd.
doi:10.1016/j.jsv.2009.03.036

values of ζ and f_1, which results in the appearance of multiple jumps. Hayashi's findings were extended in Ref. [10] for the case $\Omega \neq 1$, and for a weakly ($\gamma = 0.0783$) and strongly nonlinear system ($\gamma = 3.7033$), which are the cases relating to a configuration of a nonlinear QZS isolator [8]. In Ref. [10], the harmonic balance method (HBM) was applied to obtain the first approximation of the steady-state periodic solution. The numerical simulations showed that if ζ and γ are fixed, the number of the steady-states ranges from one to five, depending on the combinations of values of f_0 and f_1. It was also shown that combinations of f_0 and f_1 influence the number of jumps in the frequency-response curves (FRCs).

Multiple jump phenomena leading to reproducible hysteresis have been recognized in the behaviour of different nonlinear systems: the ultraharmonic resonance response of a system with an asymmetrical restoring force characteristic excited by a centrifugal exciting force [11], forced dynamics of a suspended cable [12], the response of atomic force microscopy cantilevers tapping on a sample [13], parametric resonance in electrostatically actuated microelectromechanical oscillators [14], large-amplitude vibrations of rectangular plates with geometric imperfections [15], the response of the fundamental mode shallow shells with a different shape of the boundary [16]. However, as far as the authors are aware, the appearance of these phenomena in the primary resonance response of the oscillator described by Eq. (1) has only been considered by Hayashi and in the previous work by the authors [10].

The analysis in this paper builds on that reported in Ref. [10], focusing on the influence of the constant force f_0 on the response of the system for a fixed value of the magnitude of the harmonic excitation force f_1. The main goal is to find the critical values of f_0 for which there is a change in the shape of FRCs and hence the number of jumps. In Section 2 some existing results from the literature are given with regard to their application to the system described by Eq. (1). Their limitations and deficiencies are emphasized, giving the clear reasons and motivation for this study. To help the reader, Section 3 contains some of the results given in Ref. [10], which concerns the approximate steady-state solution of Eq. (1) obtained by the HBM. In addition, in this section the corresponding stability regions are determined, as well as a bifurcation set relating to a saddle-node bifurcation. In Section 4 the effects of various values of the constant force on the response of the system are considered and a physical explanation for those effects is given. The effects of damping are analysed in Section 5. Section 6 contains conclusions. There are also two Appendices. Appendix A considers the effect of including a second harmonic on the steady-state response and also the total harmonic distortion on the primary resonance curve. Appendix B contains the Supplementary data associated with this article, which can be found in the online version.

2. On the motivation

The system with a constant and harmonic force applied and with odd geometric nonlinearity is known as the asymmetric Duffing oscillator. The asymmetric Duffing oscillator described by Eq. (1) can be transformed into another asymmetric oscillator with quadratic and cubic nonlinearity

$$z'' + 2\hat{\zeta}z' + z + \hat{\beta}z^2 + \hat{\gamma}z^3 = \hat{f}_1 \cos \hat{\Omega}\hat{t}, \tag{2}$$

where

$$z = y - \sqrt[3]{\frac{f_0}{\gamma}}, \quad \hat{\zeta} = \frac{\zeta}{\sqrt[6]{27\gamma f_0^2}}, \quad \hat{\beta} = \sqrt[3]{\frac{\gamma}{f_0}}, \quad \hat{\gamma} = \sqrt[3]{\frac{\gamma^2}{27 f_0^2}},$$

$$\hat{f}_1 = \sqrt[3]{\frac{f_1^3}{27\gamma f_0^2}}, \quad \hat{\Omega} = \frac{\Omega}{\sqrt[6]{27\gamma f_0^2}}, \quad \hat{t} = \sqrt[6]{27\gamma f_0^2}\, t \tag{3a–g}$$

with primes denoting differentiation with respect to $\hat{t}$.

The second-order method of multiple scales is used in Ref. [17] to demonstrate that a general oscillator with quadratic and cubic nonlinearity (2) has a backbone curve

$$\hat{\Omega}_{b1} = 1 - k_1 a_0^2, \quad k_1 = \frac{10\hat{\beta}^2 - 9\hat{\gamma}}{24}, \tag{4}$$

where a_0 is the steady-state amplitude of the first harmonic and $\hat{\Omega}_{b1}$ stands for the corresponding frequency. The backbone curve has only one vertical tangent, indicating that the response of the system can be either softening ($k_1 > 0$) or hardening ($k_1 < 0$).

By using Eqs. (3c) and (3d), one obtains that $k_1 = 7/24 \sqrt[3]{\gamma^2/f_0^2}$, which indicates that, regardless of the value of the constant force, the response of the oscillator (1) is softening. This conclusion is, however, misleading and it holds just for a particular ordering of the system parameters, as will be demonstrated later.

To describe correctly the dynamic behaviour of an elastic cable under planar excitation at large amplitudes, Benedettini and Rega [12] used the fourth-order method of multiple scales to obtain the expression for the backbone curve, the corresponding frequency of which is labelled by $\hat{\Omega}_{b2}$ and it is given by

$$\hat{\Omega}_{b2} = 1 - k_1 a_0^2 - k_2 a_0^4, \quad k_2 = \frac{1940\hat{\beta}^4 - 6228\hat{\beta}^2\hat{\gamma} + 405\hat{\gamma}^2}{6912}. \tag{5}$$

They found that when the cubic nonlinearity in Eq. (2) is dominant, the response is hardening with little difference to the Duffing oscillator. They also showed that, since the backbone curve (5) can have two vertical tangents, the branches of the FRC bend in such a way that the response is softening at low amplitudes and becomes hardening as the amplitude increases, with the maximum or three or five steady-state solutions.

By using Eqs. (3c) and (3d), one calculates that $k_2 = -91/6912\sqrt[3]{\gamma^4/f_0^4}$, leading to the conclusion that the backbone curve can have two vertical tangents so that, consequently, the oscillator (1) can exhibit a mixed nonlinear response. However, the conclusion found in Ref. [12] cannot be directly applied to the oscillator (1), because they refer to the elastic cable for which the coefficients of quadratic and cubic nonlinearity are mutually dependent, while the damping coefficient and the magnitude of the excitation force can have arbitrary values. By analysing the coefficients in Eqs. (3b–e) of the oscillator described by Eq. (2) corresponding to the oscillator in Eq. (1), it can be seen that all the coefficients are coupled. Thus, a more general analysis is required. This analysis is, therefore, aimed at finding the values of the constant force for which the response changes from hardening to softening, as indicated below, with all possible shapes of the FRCs, the number of steady states and jumps distinguished.

3. Amplitude–frequency response

An approximate solution corresponding to the steady-state response in the region of the primary resonance is sought by the harmonic balance method. It is assumed as the sum of a bias term and first harmonic [10] (the solution containing the second harmonic term is discussed in Appendix A)

$$y(t) = A_0 + A_1\cos(\Omega t + \theta). \tag{6}$$

Substituting Eq. (6) into Eq. (1) and equating constant terms and setting the coefficients of the terms containing $\cos\Omega t$ and $\sin\Omega t$ separately to zero, the system of coupled nonlinear algebraic equations, in terms of a bias term A_0, the amplitude of a harmonic term A_1 and phase θ is found to be

$$Y_1 \equiv \gamma A_0^3 + \frac{3}{2}\gamma A_0 A_1^2 - f_0 = 0,$$

$$Y_2 \equiv -A_1\Omega^2 + 3\gamma A_0^2 A_1 + \frac{3}{4}\gamma A_1^3 - f_1\cos\theta = 0,$$

$$Y_3 \equiv -2\zeta A_1\Omega - f_1\sin\theta = 0. \tag{7a–c}$$

Eqs. (7a–c) can be combined to give the implicit equation for the frequency-response function of A_0:

$$\sum_{i=0}^{9} b_i A_0^i = 0, \tag{8}$$

where

$$b_0 = -f_0^3, \quad b_1 = 4f_0^2\Omega^2, \quad b_2 = -4f_0\Omega^2(\Omega^2 + 4\zeta^2), \quad b_3 = 3\gamma(2f_1^2 - 3f_0^2),$$

$$b_4 = 16\gamma f_0\Omega^2, \quad b_5 = 4\gamma\Omega^2(\Omega^2 + 4\zeta^2), \quad b_6 = -15\gamma^2 f_0,$$

$$b_7 = -20\gamma^2\Omega^2, \quad b_8 = 0, \quad b_9 = 25\gamma^3. \tag{9a–k}$$

It is shown in Ref. [10] that the coefficients of the polynomial in Eq. (8) are such that for different values of ζ, γ, f_0 and f_1 the system can have a maximum number of five, three or one steady-state value for one value of frequency Ω, i.e. it can experience multi-valued steady states.

To find the *stability limits* of the steady states on the resonance curves, use can be made of the determinant $\Delta = |\partial Y_i/\partial y_j|$, where $i = 1,2,3, y_j \in \{A_0, A_1, \theta\}$, and Y_1, Y_2, Y_3 are defined by Eqs. (7a–c):

$$\Delta = -\left(3\gamma A_0^2 A_1 + \frac{3}{2}\gamma A_1^3\right)\cdot\left[\left(\Omega^2 - 3\gamma A_0^2 - \frac{3}{2}\gamma A_1^2\right)^2 - \frac{9}{16}\gamma^2 A_1^4 + 4\zeta^2\Omega^2 + \frac{6\gamma A_0^2 A_1^2\left(\Omega^2 - 3\gamma A_0^2 - \frac{3}{4}\gamma A_1^2\right)}{A_0^2 + \frac{A_1^2}{2}}\right]. \tag{10}$$

When $\Delta = 0$, there is a stability limit and a saddle-node bifurcation occurs.

The occurrence of the jumps in the system response is associated with a saddle-node bifurcation and vertical tangency of the FRC [18]. To find the locations of the vertical tangents, Eqs. (7b) and (7c) are squared and then summed to give:

$$A_1^2\cdot B = f_1^2, \tag{11}$$

where $B = (\Omega^2 - 3\gamma A_0^2 - (3/4)\gamma A_1^2)^2 + 4\zeta^2\Omega^2$.

Eq. (11) can be differentiated with respect to A_1^2 to give

$$\frac{\mathrm{d}f_1^2}{\mathrm{d}A_1^2} = \left(\Omega^2 - 3\gamma A_0^2 - \frac{3}{2}\gamma A_1^2\right)^2 - \frac{9}{16}\gamma^2 A_1^4 + 4\zeta^2\Omega^2 + \frac{6\gamma A_0^2 A_1^2\left(\Omega^2 - 3\gamma A_0^2 - \frac{3}{4}\gamma A_1^2\right)}{A_0^2 + \frac{A_1^2}{2}}. \tag{12}$$

Since $\mathrm{d}f_1^2/\mathrm{d}A_1^2 = \sqrt{B}(\mathrm{d}f_1/\mathrm{d}A_1)$, if Eq. (12) is equal to zero, then $\mathrm{d}f_1/\mathrm{d}A_1$ is also equal to zero. Further, it has been shown that the last condition implies $\mathrm{d}\Omega/\mathrm{d}A_1 = 0$, which is the condition for a vertical tangent (see, for example, [9]). Thus, setting Eq. (10) to zero defines the condition for a vertical tangent. Comparing Eq. (12) with Eq. (10), it is seen that if the expression in Eq. (12) is equal to zero, then $\Delta = 0$. This confirms that the FRC has a vertical tangent at the stability limits, where saddle-node bifurcations occur. When these limits are known, stable and unstable parts of the regions of FRCs between two vertical tangents are determined from the stability condition for the second unstable region of the linearized variational equation, which has the form of Hill's equation [10].

The approximate saddle-node bifurcation set in terms of f_0 and Ω, when the other parameters are fixed, is calculated from Eqs. (7a–c) and shown in Fig. 1a. It consists of two pairs of bifurcation curves: BA and AC, meeting at a cusp bifurcation point A, and QP and PR, meeting at the other cusp P. These bifurcation curves indicate how the fixed points are created or annihilated. The change in the number of the fixed points is also denoted in this figure. On the curves AB and QS (red solid line) the saddle-node bifurcation occurs that corresponds to the coalescence of two fixed points (one stable and one unstable) when one fixed point exists. Their disappearance is related to the curve AS, TC, and RT (red dashed line). The curve SP (blue dotted line) depicts the situation when there is a bifurcation from three fixed points (two stable and one unstable) to five (three stable and two unstable). Along ST and TP (blue dashed–dotted line) the opposite holds—one stable and one unstable fixed point disappear. At the cusps A and P, a further degeneracy occurs and there is a multiply repeated

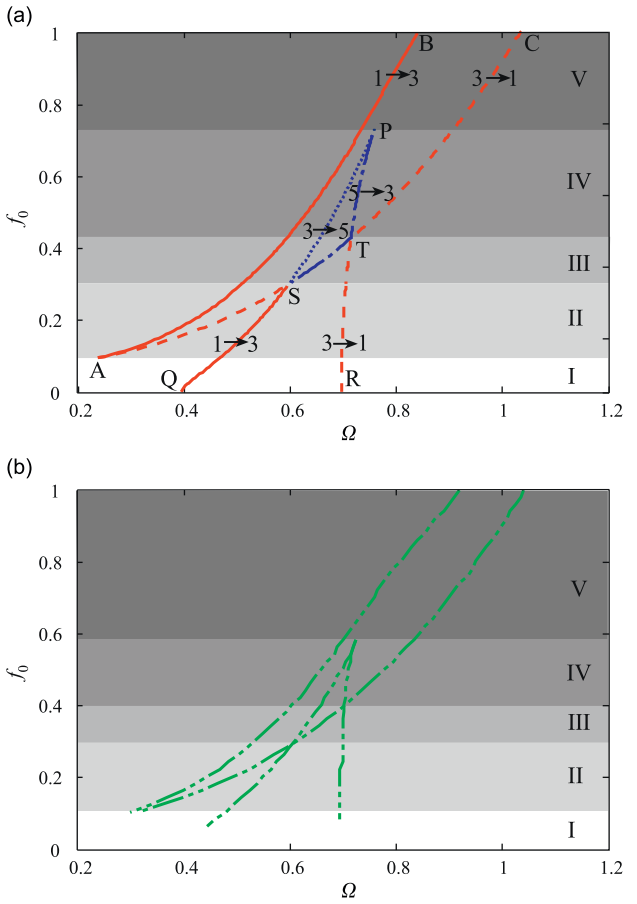

Fig. 1. (a) An approximate saddle-node bifurcation set in the (Ω, f_0) plane for $\zeta = 0.025$, $\gamma = 0.0783$ and $f_1 = 0.1$: bifurcation from one to three fixed points (red solid line), bifurcation from three to one fixed point (red dashed line), bifurcation from three to five fixed points (blue dotted line) and bifurcation from five to three fixed points (blue dashed–dotted line). Regions labelled by I–V correspond to the Cases analysed in Section 4 and (b) a numerically computed saddle-node bifurcation set (green line – · · –). (For interpretation of the references to the colour in this figure legend, the reader is referred to the web version of this article.)

root. Fig. 1b shows saddle-node bifurcation curves computed numerically. They confirm that the behaviour of the system is captured reasonably well by the theoretical results given in Fig. 1a. Generally, Fig. 1 indicates that depending on the values of f_0 there can be from two to four saddle-node bifurcations and the system can experience two to four jumps. Depending on this number and the maximum number of steady states and the number of jumps when frequency is increased or decreased quasi-statically, the (Ω, f_0) plane in Fig. 1 is divided into five regions labelled by I–V. The shapes of the FRCs relating to them are considered in the next section.

4. On the shape of the FRCs

4.1. Influence of the value of the constant force on the shape of the FRCs

To illustrate how the value of the constant force affects the shape of FRCs, these curves are plotted in Figs. 2–6 for five distinguishable cases (Case I–V). The magnitude of harmonic excitation is held fixed $f_1 = 0.1$, as are the parameters $\zeta = 0.025$ and $\gamma = 0.0783$, while the value of the constant force is increased. In order to assure a consistent accuracy of an assumed solution obtained by the HBM, the combinations of parameters are chosen in such a way that they lead to the response in which higher harmonics are negligible in comparison to that given in Eq. (6). The results from the stability analysis are also shown in Figs. 2–6, where the dashed parts of the FRCs represent the unstable regions. In addition, the equation of motion (1) was solved numerically and the bias term, and the amplitude and phase of the first harmonic were calculated from the Fourier series coefficients of the steady-state response. They are depicted in Figs. 2–6 as circles, confirming that the analytical results qualitatively capture the behaviour of the system. An additional quantitative confirmation of the validity of the assumed solution is given in Appendix A, which discusses the effect of including the second harmonic in the response and the total harmonic distortion. The dashed–dotted lines in Figs. 2–6 are for the primary resonance curve when it is assumed that the solution consists of two harmonics, named as 'the solution by the HBMS'.

When the constant force is very small, which corresponds to Case I where $f_0 = 0.01$, the FRC of the harmonic response is bent to the right (Fig. 2), as is for a hardening Duffing oscillator [17]. The occurrence of one jump when the frequency is increased or decreased quasi-statically can be seen. When the harmonic term experiences a jump-down, the bias term experiences a jump-up and vice-versa. These jumps illustrate possible saddle-node bifurcations that can be detected from Fig. 2. The intersection of the horizontal line $f_0 = 0.01$ with the curves QS or RT enables one to predict the frequency at which there is a jump in the response.

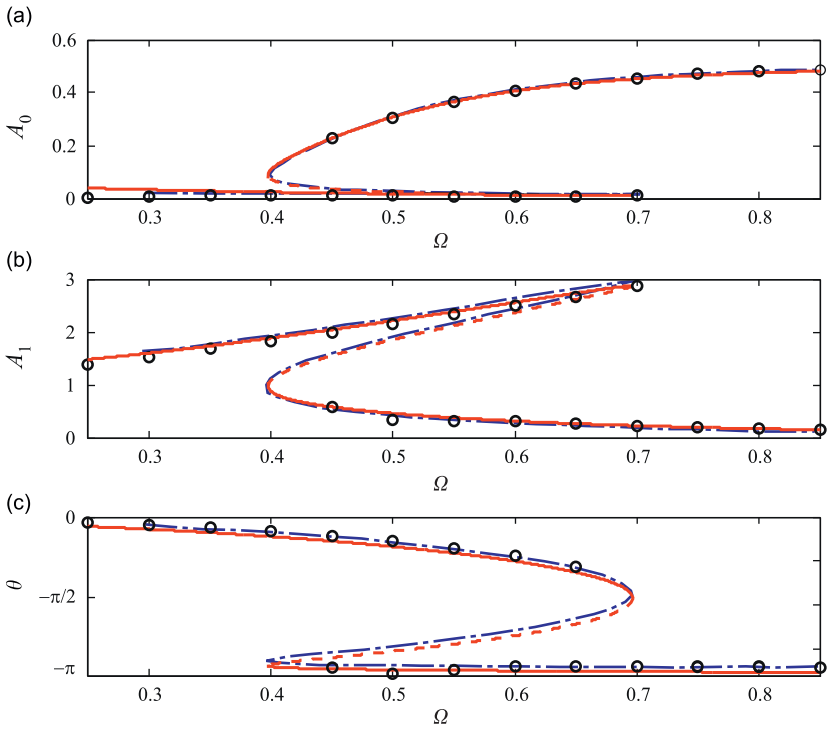

Fig. 2. Frequency-response curves of: (a) the bias term A_0, (b) harmonic term A_1 and (c) phase θ, for the Case I, corresponding to $\zeta = 0.025$, $\gamma = 0.0783$, $f_1 = 0.1$ and $f_0 = 0.01$; '–' stable solution by the HBM; '– –' unstable solution by the HBM; 'o' numerical solution; '· – · –' solution by the HBMS.

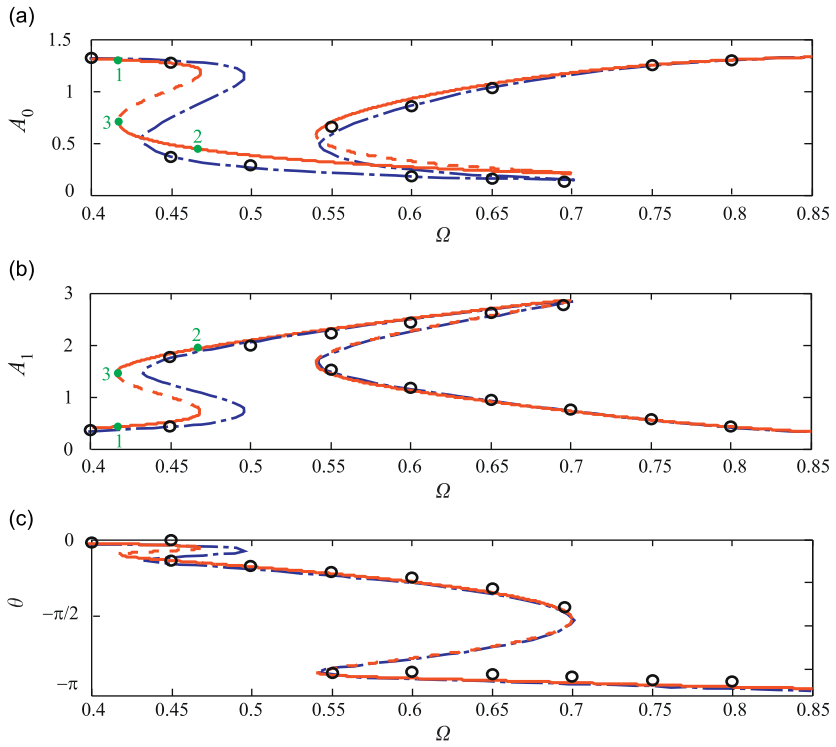

Fig. 3. Frequency-response curves of: (a) the bias term A_0, (b) harmonic term A_1 and (c) phase θ, for the Case II, corresponding to $\zeta = 0.025$, $\gamma = 0.0783$, $f_1 = 0.1$ and $f_0 = 0.2$; '–' stable solution by the HBM; '– –' unstable solution by the HBM; 'o' numerical solution; '· – · –' solution by the HBMS. Points 1–3 refer to the analysis given in Section 4.2 and Fig. 8.

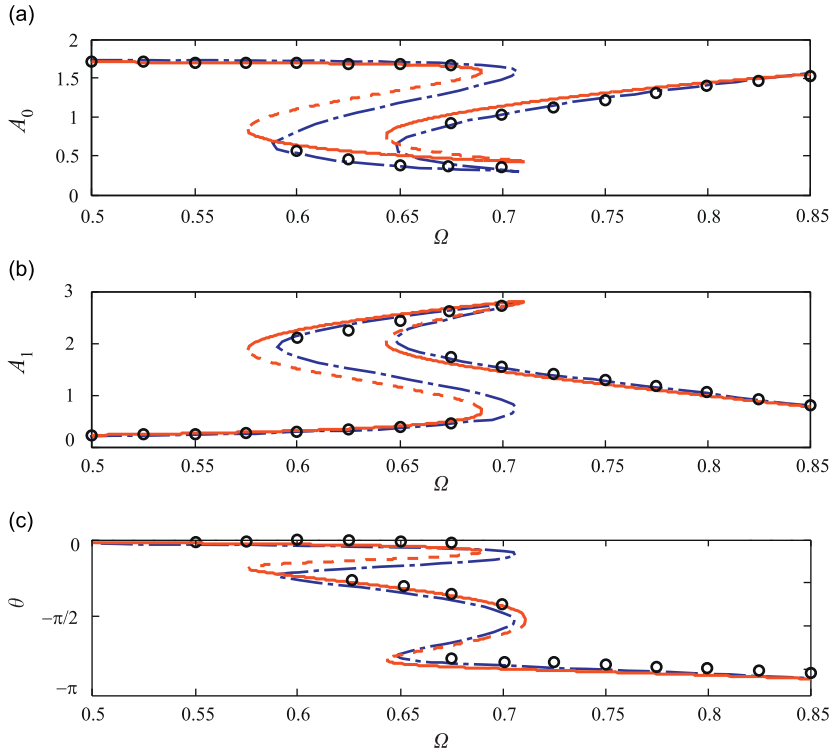

Fig. 4. Frequency-response curves: (a) the bias term A_0, (b) harmonic term A_1 and (c) phase θ, for the Case III, corresponding to $\zeta = 0.025$, $\gamma = 0.0783$, $f_1 = 0.1$ and $f_0 = 0.4$; '–' stable solution by the HBM; '– –' unstable solution by the HBM; 'o' numerical solution; '· – · –' solution by the HBMS.

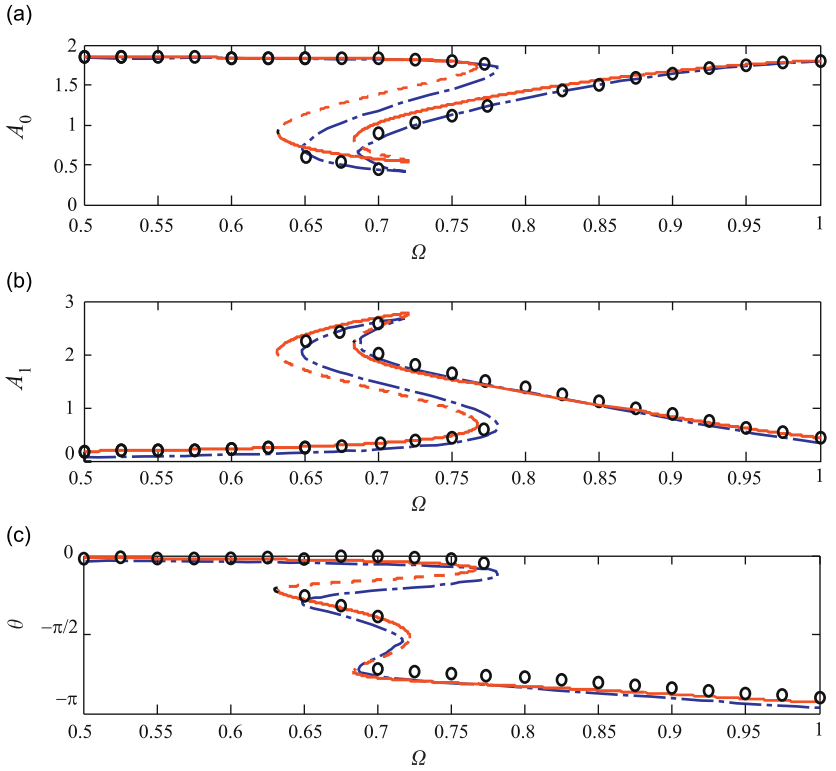

Fig. 5. Frequency-response curves: (a) the bias term A_0, (b) harmonic term A_1 and (c) phase θ, for the Case IV, corresponding to $\zeta = 0.025$, $\gamma = 0.0783$, $f_1 = 0.1$ and $f_0 = 0.5$; '–' stable solution by the HBM; '– –' unstable solution by the HBM; 'o' numerical solution; '· – · –' solution by the HBMS.

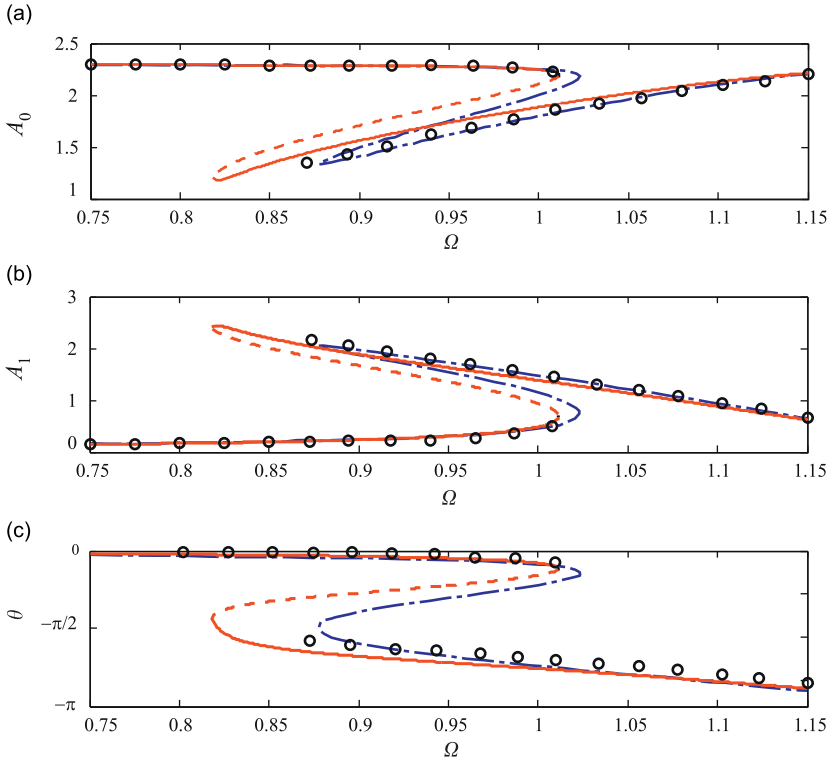

Fig. 6. Frequency-response curves: (a) the bias term A_0, (b) harmonic term A_1 and (c) phase θ, for the Case V, corresponding to $\zeta = 0.025$, $\gamma = 0.0783$, $f_1 = 0.1$ and $f_0 = 0.95$; '–' stable solution by the HBM; '– –' unstable solution by the HBM; 'o' numerical solution; '· – · –' solution by the HBMS.

When the constant force is increased to $f_0 = 0.2$, a markedly different shape of FRC is observed (Fig. 3), corresponding to Case II. The upper branch of the FRC of the harmonic response bends first to the left, experiencing a softening effect and then to the right experiencing a hardening effect. Thus, the system experiences four jumps in its response: two jumps occur when increasing frequency and two jumps when decreasing frequency. As a consequence, the system exhibits hysteretic behaviour.

The FRCs for $f_0 = 0.4$, which is labelled as Case III, are given in Fig. 4. The upper branch of the FRC of the harmonic response bends even more to the left, while the jump-up and jump-down points move towards higher frequencies. The additional feature of this case is that there is a frequency region where five steady states exist. It corresponds to the frequency range between the curves SP and ST in Fig. 1.

The FRCs corresponding to Case IV for which $f_0 = 0.5$ are shown in Fig. 5. They are characterized by the fact that there is a region of frequency for which five steady states exist, which corresponds to the frequency range between the curves SP and TP in Fig. 1. In addition, it should be noted that the value of the jump-up frequency of the harmonic term on the left branch is higher than the frequency at which the peak amplitude occurs. The system can exhibit one jump when the frequency is increased and two jumps when it is decreased.

Finally, when the value of the constant force is significantly increased to $f_0 = 0.95$, the FRC of the harmonic response is bent to the left in a similar way to the response of a softening Duffing oscillator [17]. This Case V is plotted in Fig. 6. Again, the system has one jump-up and one jump-down frequency.

To help the reader to visualize how the FRCs change from one typical shape to another one, an animation has been created. The animation can be viewed in Supplementary data associated with this article in its online version the details of which can be found in Appendix B.

4.2. The role of instantaneous stiffness on the shape of the FRCs

Eq. (7a) can be written as

$$1 + \frac{3}{2}\frac{A_1^2}{A_0^2} - \frac{f_0}{\gamma A_0^3} = 0. \tag{13}$$

The value of A_0 at the frequency when the behaviour changes from softening to hardening (point 3 in Fig. 3) is the same as when the backbone curve of the bias term changes from having a negative gradient to a positive gradient (see Fig. 3 in Ref. [10]). The backbone curve for the bias term is given by Eq. (11) in Ref. [10], which is

$$\Omega_{b0}^2 = \frac{5\gamma}{2}A_0^2 + \frac{f_0}{2A_0}. \tag{14}$$

The value of A_0 required, can be determined by setting $\mathrm{d}\Omega_{b0}/\mathrm{d}A_0 = 0$ and solving to give

$$\frac{f_0}{\gamma} = 10A_0^3. \tag{15}$$

Substituting for f_0/γ from Eq. (15) into Eq. (13) and rearranging gives

$$\frac{\sqrt{6}A_0}{A_1} = 1. \tag{16}$$

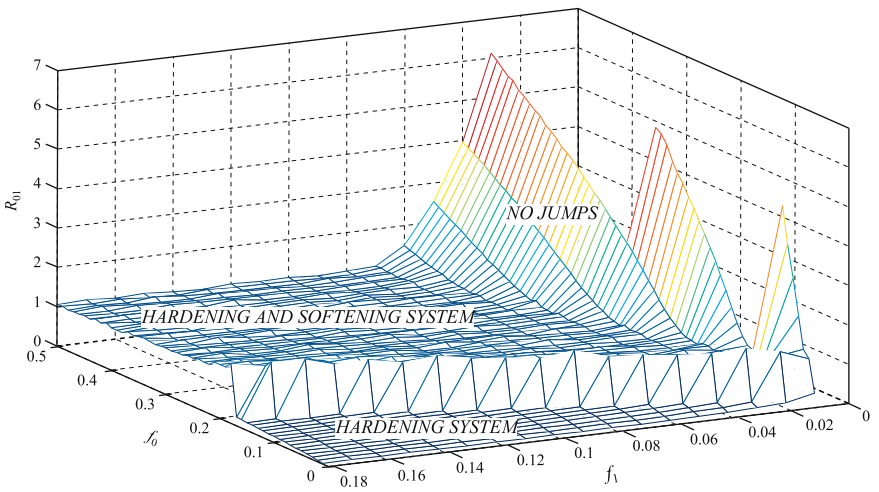

Fig. 7. The value of the ratio $R_{01} = \sqrt{6}A_0/A_1$ evaluated at the frequency when the characteristic of the FRC changes from being softening to hardening. This is given by point 3 in Fig. 3.

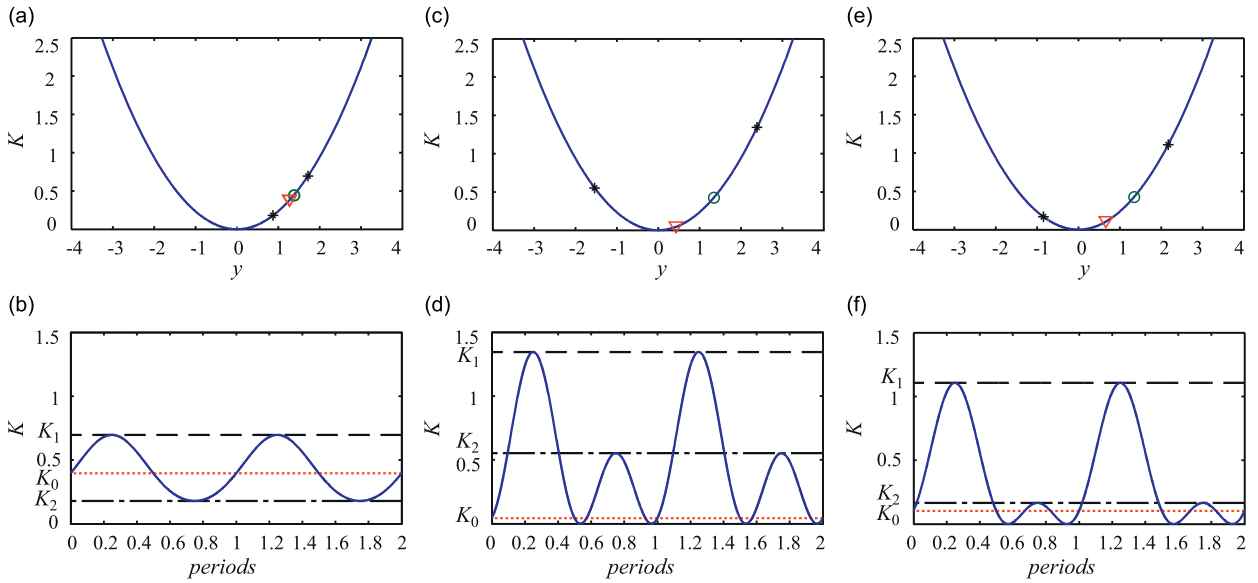

Fig. 8. Graphs showing how the non-dimensional stiffness changes as a function of displacement: (a) point 1 in Fig. 3, (c) point 2 in Fig. 3 and (e) point 3 in Fig. 3. 'o' denotes the static displacement, '∇' denotes the displacement A_0 due to the force f_0 and '*' the peak displacement either side of A_0. Figs. (b), (d) and (e) are the corresponding time histories of the stiffness over two cycles, K_0 is the non-dimensional stiffness corresponding to point '∇' and K_1, K_2 corresponding to the peak displacements either side of A_0 given by '*'.

The value of $R_{01} = \sqrt{6}A_0/A_1$ was calculated numerically for $f_0 \in [0, 0.5]$ and $f_1 \in [0, 0.2]$ and is shown in Fig. 7. Three regions are shown in the figure; the region where $R_{01} \approx 1$, which corresponds to when there is a change in the characteristic from softening to hardening; the region when the harmonic displacement A_1 is too small for a jump to occur; the region where the system has only hardening behaviour.

To investigate further why asymmetry causes the characteristic of softening for low amplitudes of vibration and hardening behaviour for large amplitudes of vibration, the instantaneous stiffness of the system is studied. Three cases are examined corresponding to points 1, 2 and 3 in Fig. 3; the first is when the system has softening behaviour (point 1), the second when the system has hardening behaviour (point 2) and the third when the system is on the boundary between softening and hardening behaviour (point 3). The non-dimensional stiffness of the system for these cases is shown in Figs. 8a, c and e. In these figures 'o' denotes the static displacement, '∇' the displacement A_0 due to the force f_0 and '*' the peak displacement either side of A_0. The corresponding instantaneous non-dimensional stiffnesses are given in Figs. 8b, d and f. The stiffness of the system due to the bias term is given by

$$K_0 = 3\gamma A_0^2. \tag{17}$$

and the instantaneous stiffness at the extreme positions are given by

$$K_{1,2} = 3\gamma(A_0 \pm A_1)^2. \tag{18a,b}$$

In the case shown in Fig. 8a, $A_1 < A_0$, and as shown in Fig. 8b, the stiffness of the system increases compared to the stiffness due to the bias term over one half of the cycle and reduces over the other half of the cycle. In this case the system behaves as a softening system. In the second case, shown in Figs. 8c and d, $A_1 > \sqrt{6}A_0$. In one half of the cycle the stiffness of the system increases compared to the stiffness due to the bias term; in the other half of the cycle the stiffness first reduces until it reaches zero, then it increases again until at its peak it is much larger than that due to the bias term alone. This system behaves as a hardening system. In the third case shown in Figs. 8e and f, the system is on the boundary between the softening system and the hardening system which requires that $A_1 = \sqrt{6}A_0$.

The threshold instantaneous stiffness at the extreme position can be determined relatively easily. The instantaneous stiffness at the extreme position of interest is given by Eq. (18b). Combining Eqs. (16)–(18b) gives the ratio of the stiffness at the extreme position to that at the bias position when the system changes its characteristic from being softening to hardening

$$\frac{K_2}{K_0} = (1 - \sqrt{6})^2 \approx 2.1. \tag{19}$$

Thus if the stiffness at the extreme position (having passed through zero) is about twice the stiffness due to the bias term alone then the system will behave as a hardening system.

5. Influence of damping on the response of the system

5.1. The decrease of damping

In order to illustrate the influence of the decrease of damping on the shape of the bifurcation sets, they are plotted for $\zeta = 0.0125$ (Fig. 9a) and $\zeta = 0.00625$ (Fig. 9b). Both parts of the figure are plotted for $\gamma = 0.0783$, $f_1 = 0.1$, and contain the bifurcation sets obtained analytically (the legend is the same as that explained in Section 3 and below Fig. 1). It should be noted that the bifurcation sets were also obtained numerically. Being very similar to the analytical ones, they are not shown in order not to make Figs. 9 and 10 cluttered. It can be seen that the structure of the bifurcation sets shown in Fig. 9 is the same as the one given in Fig. 1, with two pairs of bifurcation curves and two cusps. Because of that, all five cases labelled in Fig. 1 can also be identified in Fig. 9, and scenarios of the appearance of jumps are equal to those described above. It can also be noted that the left pair of curves and the corresponding cusp given in Fig. 9a slightly change with the decrease of damping, while the right pair is more affected. The left curve of this pair comes closer to the left branch of the other pair, or, in other words, the curve QP from Fig. 1 becomes closer to the curve AB from the same figure. It indicates that the frequencies at which jump-down and jump-up occur are closer to each other. The right curve from the right pair is almost vertical, which means that the corresponding jump occurs at approximately the same frequency regardless of the values the constant force: at $\Omega \approx 1$ for $\zeta = 0.0125$ (see Fig. 9a) and at $\Omega \approx 1.4$ for $\zeta = 0.00625$ (see Fig. 9b). With the reduction of damping its cusp moves toward higher frequencies and higher values of the magnitude of the constant force. In the special case, when damping is zero, it goes to infinity, since two branches of the FRC do not meet. As a result, the curve PR from Fig. 1 shifts to the right-hand side, to infinity.

5.2. The increase of damping

The bifurcation sets illustrating the effects of the increase of damping on the onset of saddle-node bifurcations are given in Fig. 10a for $\zeta = 0.05$ and in Fig. 10b for $\zeta = 0.075$. The rest of the parameters are held fixed at their previous values.

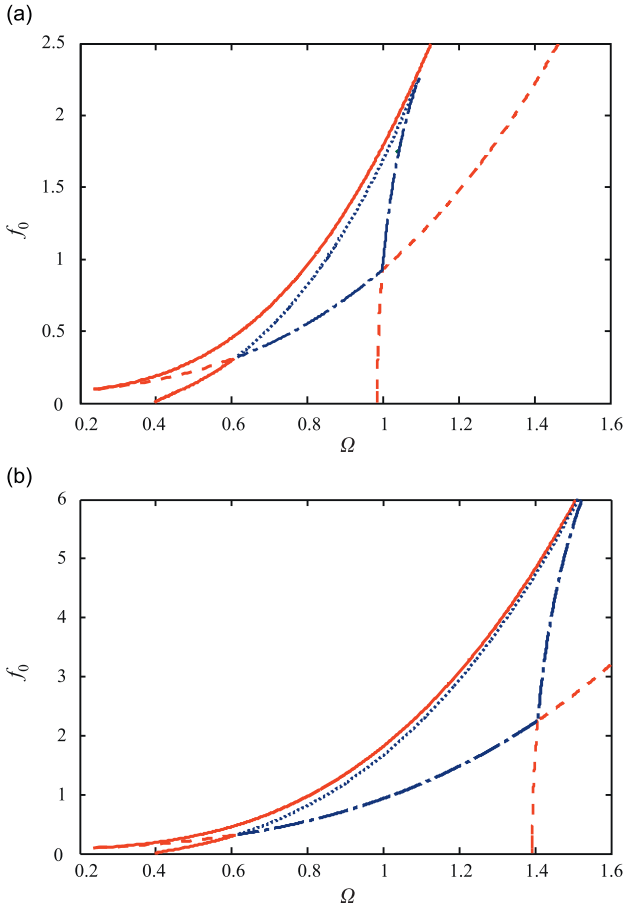

Fig. 9. An approximate analytical saddle-node bifurcation set in the (Ω, f_0) plane for $\gamma = 0.0783, f_1 = 0.1$: (a) $\zeta = 0.0125$ and (b) $\zeta = 0.00625$. Legend as in Fig. 1.

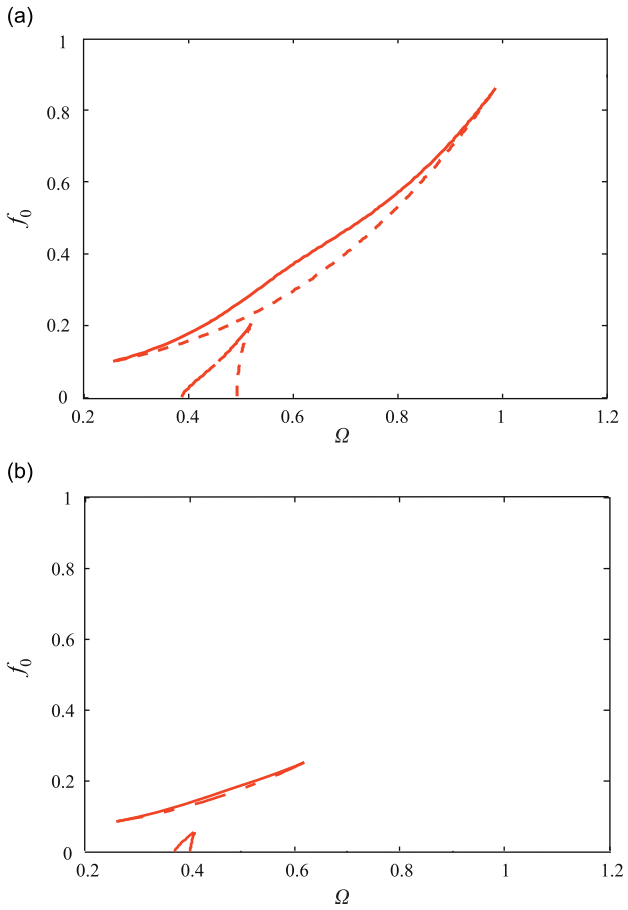

Fig. 10. An approximate analytical saddle-node bifurcation set in the (Ω, f_0) plane for $\gamma = 0.0783, f_1 = 0.1$: (a) $\zeta = 0.05$ and (b) $\zeta = 0.075$. Legend as in Fig. 1.

Comparing these figures mutually as well as with the bifurcation set given in Fig. 1, it can be concluded that the basic bifurcation structure is crucially dependent on this change in the value of the damping ratio. First, the pairs of bifurcation curves do not intersect each other, i.e. one does not cross over into the frequency region where the others occur. Consequently, there is no region corresponding to five steady states, which implies that making the damping ratio higher reduces the maximum number of the steady states. Second, the regions between the branches of each pair narrow down. Finally, Fig. 10b shows that if the damping ratio is increased appropriately, there is only a small range of the values of the constant force for which jumps can occur. For the majority of the values of the constant force from the range investigated, there is no saddle-node bifurcation, i.e. the system does not experience jump phenomena, but does exhibit linear-like behaviour, with FRCs that are single-valued functions. This implies that a suitable choice of damping can be used as a passive mechanism to eliminate the occurrence of jumps in the system.

5.3. *On the location of the upper cusp*

It has been noted in Section 5.1 that the location of the lower cusp, which corresponds to the jump-down point on the left branch of the FRC of the harmonic term, is slightly affected if damping is changed for the fixed values of the coefficient of nonlinearity and the magnitude of harmonic excitation. However, the location of the upper cusp is affected more significantly if the same change occurs. It was shown in Ref. [19] that the frequency corresponding to the jump-down point of a classic Duffing oscillator actually depends on the ratio between the coefficient of nonlinearity and the square of the damping ratio. To examine this dependence for the case of the asymmetric Duffing oscillator, the frequency corresponding to upper cusp is calculated numerically for several values of the coefficient of nonlinearity ($\gamma = 0.05$; 0.0783 and 0.1) and several values of the damping ratio ($\zeta = 0.0125$; 0.025; 0.05; 0.1 and 0.15). The results are presented as a function of the ratio γ/ζ^2 in Fig. 11. The coinciding curves confirm that this jump-down frequency is dependent not only on the parameter of nonlinearity γ, but upon the ratio γ/ζ^2.

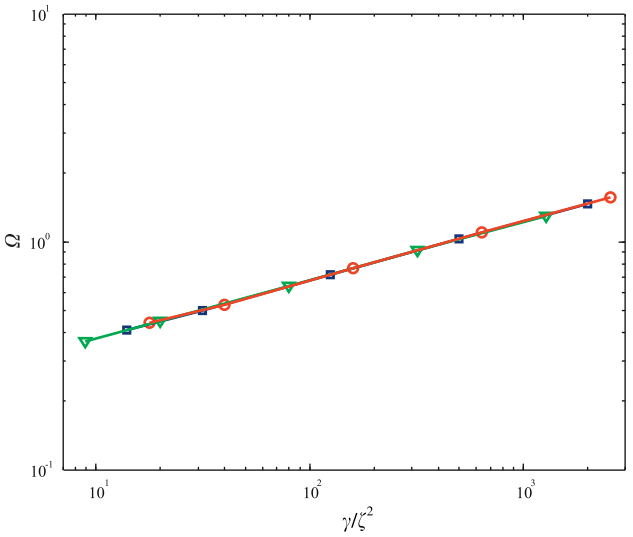

Fig. 11. The frequency corresponding to the upper cusp calculated for several values of the coefficient of nonlinearity $\gamma = 0.05$ (red circle), $\gamma = 0.0783$ (blue square) and $\gamma = 0.1$ (green triangle) and several values of the damping ratio ($\zeta = 0.0125$; 0.025; 0.05; 0.1 and 0.15). In all cases $f_1 = 0.1$. (For interpretation of the references to the colour in this figure legend, the reader is referred to the web version of this article.)

6. Conclusions

The primary resonance response of a QZS single-dof oscillator subject to simultaneous constant and harmonic excitation has been considered. The harmonic balance method was applied to determine the frequency-response equations. The stability condition of the steady-state solution was obtained, as well as the approximate bifurcation set corresponding to a saddle-node bifurcation. Numerical simulations confirmed that, although a relatively simple analytical approximation was assumed, it was sufficient to capture the fundamental response of the system. It was found that the constant external force causes asymmetry in the system, which results in the frequency-response curves having several different shapes depending on the degree of asymmetry. When the constant force is very small or very large compared to the harmonic force, the peak of the harmonic response is bent in a single direction—to the right or to the left, as it is for the response of a hardening or softening Duffing oscillator. For the values of the constant force between these extreme cases, some distinctive shapes of the frequency-response curves can occur. The upper branch of the harmonic response can have a double bend. First, it bends towards lower frequencies, experiencing initial softening. Then it bends towards higher frequencies, exhibiting subsequent hardening. These double bends can be with three or five steady-state values. The multi-valuedness of these curves causes the occurrence of the multiple jumps in the system and hysteretic behaviour. However, the system does not exhibit a jump phenomenon if the damping is high enough.

Acknowledgement

This study has partly been financially supported by the Ministry of Science, Republic of Serbia (Project no. 144008) as well as the Royal Society, UK/International Joint Project 'Using nonlinearity to improve the performance of vibrating systems'.

Appendix A. On the consistency of the assumed solution

The equation of motion of the QZS oscillator (1) can be transformed into the equation with the quadratic and cubic nonlinearity (see Section 2). It is shown in Ref. [17] that the quadratic nonlinearity brings the second harmonic into a primary resonance response. Knowing this fact, one can assume that the solution of Eq. (1) contains the second harmonic as well

$$y = A_0 + A_1 \cos(\Omega t + \theta) + A_2 \cos(2\Omega t + \varphi). \tag{A.1}$$

By using the harmonic balance method, the unknown variables A_0, A_1, A_2, φ and θ are found to satisfy (they are referred to as 'solutions obtained by the HBMS'):

$$\gamma A_0^3 + \frac{3}{2}\gamma A_0 A_1^2 + \frac{3}{2}\gamma A_0 A_2^2 + \frac{3}{4}\gamma A_2 A_1^2 \cos(\varphi - 2\theta) - f_0 = 0,$$

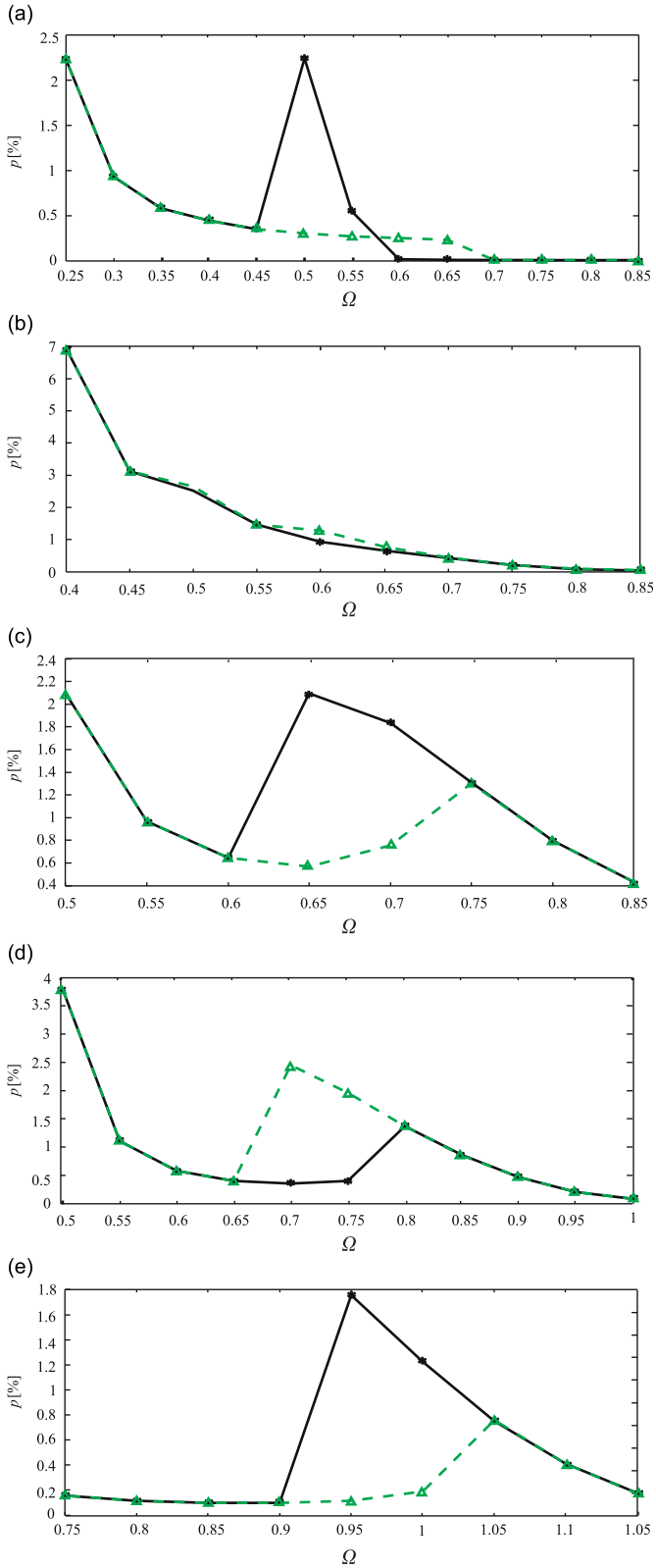

Fig. 12. The total harmonic distortion p (%), where 'Δ' labels the total harmonic distortion when increasing the frequency; '*' labels the total harmonic distortion when decreasing the frequency: (a) Case I, (b) Case II, (c) Case III, (d) Case IV and (e) Case V.

$$A_1\Omega^2 - \frac{3}{4}\gamma A_1^3 - 3\gamma A_0^2 A_1 - 3\gamma A_0 A_1 A_2 \cos(\varphi - 2\theta) - \frac{3}{2}\gamma A_1 A_2^2 + f_1 \cos\theta = 0,$$

$$2\zeta A_1\Omega + 3\gamma A_0 A_1 A_2 \sin(\varphi - 2\theta) + f_1 \sin\theta = 0,$$

$$4A_2\Omega^2 - \frac{3}{4}\gamma A_2^3 - 3\gamma A_0^2 A_2 - \frac{3\gamma}{2} A_0 A_1^2 \cos(2\theta - \varphi) - \frac{3}{2}\gamma A_1^2 A_2 = 0,$$

$$4\zeta A_2\Omega + \frac{3\gamma}{2} A_0 A_1^2 \sin(2\theta - \varphi) = 0. \tag{A.2}$$

However, the approximate steady-state solution (6) of Eq. (1) is assumed in this paper as containing the first harmonic only. Its consistency might be considered as questionable because of what is known *a priori* about the response.

In order to address this issue, Eqs. (A.2) are solved numerically for all five characteristic cases analysed in Section 4.1. The results are shown in Figs. 2–6, together with the solutions obtained by using the first harmonic term only and the corresponding equations (7a–c). It can be seen that the solutions obtained by the HBMS do not change the jump frequencies on the right-hand side branches of the FRCs significantly. They do influence more the jump frequencies on the left-hand side branches which are related to the softening behaviour and the effect of the quadratic term discussed above. As a result of that, the corresponding saddle-node bifurcation set would be shifted slightly, but all five distinguishable cases would still be recognized as in Fig. 1. This implies that the solution obtained by using the first harmonic term (6) can be considered as an accurately consistent approximation as it qualitatively captures the behaviour of the system. Quantitatively, it also gives reasonably accurate results, which is illustrated in Fig. 12. These graphs show the total harmonic distortion for Cases I–V. The total harmonic distortion is defined as the total signal power in all the harmonic distortion components divided by the power in the fundamental frequency, as a percentage p (%). From the numerical time domain simulation, using ode45, this is estimated from $\sum_{k=2}^{N} |A_k|^2 / A_1^2$, where A_k is the Fourier series coefficient of the kth harmonic and N the number of harmonics obtained, which is determined by the Nyquist frequency, which was set at 32 in this case. The low level of distortion obtained was assured by a careful choice of the values of the system parameters.

Appendix B. Supplementary material

Supplementary data associated with this article can be found in the online version at 10.1016/j.jsv.2009.03.036.

References

[1] P. Alabuzhev, A. Gritchin, L. Kim, G. Migirenko, V. Chon, P. Stepanov, *Vibration Protecting and Measuring Systems with Quasi-Zero Stiffness*, Hemisphere Publishing, New York, 1989.
[2] P. Lorrain, Low natural frequency vibration isolator or seismograph, *Review of Scientific Instruments* 45 (1974) 198–202.
[3] L. Lacoste, Lacoste and Romberg straight-line gravity meter, *Geophysics* 48 (1983) 606–610.
[4] D.L. Platus, Negative-stiffness-mechanism vibration isolation systems. SPIE—vibration control in microelectronics, *Optics and Metrology* 1619 (1991) 44–54.
[5] B. Ravindra, A.K. Mallik, Performance of nonlinear vibration isolators under harmonic excitation, *Journal of Sound and Vibration* 170 (1994) 325–337.
[6] J.T. Xing, Y.P. Xiong, W.G. Price, Passive–active vibration isolation systems to produce zero or infinite dynamic modulus: theoretical and conceptual design strategies, *Journal of Sound and Vibration* 286 (2005) 615–636.
[7] I.J. Sokolov, V.I. Babitsky, N.A. Halliwell, Hand-held percussion machines with low emission of hazardous vibration, *Journal of Sound and Vibration* 306 (2007) 59–73.
[8] I. Kovacic, M.J. Brennan, T.P. Waters, A study of a non-linear vibration isolator with a quasi-zero stiffness characteristic, *Journal of Sound and Vibration* 135 (3) (2008) 700–711.
[9] C. Hayashi, *Nonlinear Oscillations in Physical Systems*, McGraw-Hill, New York, 1964.
[10] I. Kovacic, M.J. Brennan, B. Lineton, On the resonance response of an asymmetric Duffing oscillator, *International Journal of Non-Linear Mechanics* 43 (9) (2008) 858–867.
[11] W. Carnegie, Z.F. Reift, Ultraharmonic resonance of a system with an asymmetrical restoring force characteristic, *Journal of Mechanical Engineering Science* 11 (1969) 592–597.
[12] F. Benedettini, G. Rega, Non-linear dynamics of an elastic cable under planar excitation, *International Journal of Non-Linear Mechanics* 22 (6) (1987) 497–509.
[13] S.I. Lee, S.W. Howell, A. Raman, R. Reifenberger, Nonlinear dynamics of microcantilevers in tapping mode atomic force microscopy: a comparison between theory and experiment, *Physical Review B* 66 (2002) 115409.
[14] J.F. Rhoads, S.W. Shaw, K.L. Turner, J.B. Moehlis, E. DeMartini, W. Zhang, Generalized parametric resonance in electrostatically actuated microelectromechanical oscillators, *Journal of Sound and Vibration* 296 (2006) 797–829.
[15] M. Amabili, Theory and experiments for large-amplitude vibrations of rectangular plates with geometric imperfections, *Journal of Sound and Vibration* 291 (2006) 539–565.
[16] L. Kurpa, G. Pilgun, M. Amabili, Nonlinear vibrations of shallow shells with complex boundary: R-functions method and experiments, *Journal of Sound and Vibration* 306 (2007) 580–600.
[17] A.H. Nayfeh, D.T. Mook, *Nonlinear Oscillations*, Wiley, New York, 1979.
[18] A.H. Nayfeh, B. Balachandran, *Applied Nonlinear Dynamics*, Wiley, New York, 1994.
[19] M.J. Brennan, I. Kovacic, A. Carrella, T.P. Waters, On the jump-up and jump-down frequencies of the Duffing oscillator, *Journal of Sound and Vibration* 318 (2008) 1250–1261.